CAUCHY – Jurnal Matematika Murni dan Aplikasi
Volume 11 (2) (2026), Pages 2026–2043
p-ISSN: 2086-0382; e-ISSN: 2477-3344

Optimal Control of a Forest Resource Model Under Population Growth and Mining Activities

Asmaidi[1,3], Fatmawati*[2], and Cicik Alfiniyah[2]

[1] *Doctoral Program of Mathematics and Natural Sciences, Faculty of Science and Technology, Universitas Airlangga, Surabaya 60115, Indonesia*
[2] *Department of Mathematics, Faculty of Science and Technology, Universitas Airlangga, Surabaya 60115, Indonesia*
[3] *Department of Mathematics, Faculty of Mathematics and Natural Sciences, Mulawarman University, Samarinda, 75123, Indonesia*

Abstract

Forest resources sustain essential ecological functions, while population pressure and mining activity can accelerate forest degradation. This study develops an optimal-control extension of an established forest–population-pressure–mining framework by introducing two bounded intervention efforts: environmental education and mining restriction. Forest condition, human population, population pressure, and mining activity are represented as dimensionless model indices on an arbitrary illustrative scenario scale; therefore, the numerical states are not obtained from normalized empirical observations. The objective functional rewards the forest index and penalizes population pressure, mining activity, and quadratic intervention effort. The analysis establishes local well-posedness, positivity, a valid positively invariant region, global continuation, a control-dependent equilibrium for constant interventions, and the existence of an optimal control. A new comparative-statics result shows that, whenever the positive constant-control equilibrium exists, its forest component increases strictly with either intervention. Reproducible supplementary code supports the baseline and extended sensitivity calculations. Three time-grid tests yield stable results, while a four-start direct single-shooting control-parameterization diagnostic produces objective values differing by approximately 0.074% from the forward–backward sweep candidate. Under the illustrative baseline, the two-control candidate gives the lowest computed aggregate objective and the highest terminal forest index, whereas education-only control gives the lowest terminal population-pressure index. These findings remain model- and weight-dependent, not location-specific causal or economic policy estimates.

Keywords: Dynamic model; forest resources; mining activities; optimal control; population pressure.

1. Introduction

Forests provide ecological regulation, carbon storage, biodiversity habitat, and livelihood support [1–3]. Demographic and extractive processes can affect forest condition through several interacting pathways. Mining is one direct source of forest loss in particular settings, whereas the relative

***Corresponding author**. E-mail: fatmawati@fst.unair.ac.id

Received: June 4, 2026 Revised: August 12, 2026 Accepted: September 1, 2026
DOI: https://doi.org/10.18860/cauchy.v11i2.44782

importance of mining, agriculture, infrastructure, and other drivers is context dependent [4, 5]. A pantropical assessment has documented substantial direct and indirect forest loss associated with industrial mining, although its magnitude varies considerably among countries [6]. These interactions motivate a dynamic model of forest-resource condition, human population, population pressure, and mining activity [7].

An established four-state nonlinear framework has examined population-induced mining pressure on forest resources [8]. Recent mathematical studies similarly represent human population and population pressure as important drivers of forest-biomass dynamics, while emphasizing the effects of simplifying assumptions and parameter uncertainty [9]. The present study retains that state structure and formulates a bounded optimal-intervention problem. Environmental education and mining restriction are represented as stylized channels that increase the removal rates of population pressure and mining activity, respectively. The study introduces neither a new empirical forest dataset nor an economic equilibrium model; it gives a mathematically consistent numerical analysis of a dimensionless-index system. Related recent research has combined a nonlinear CO_2–forest-biomass–temperature model with real-data parameter estimation, sensitivity analysis, reforestation control, and cost-effectiveness analysis. Unlike that climate-oriented study, which considers private-vehicle access limitation and reforestation, the present study examines population pressure and mining activity through stylized environmental-education and mining-restriction channels [10].

The revised formulation makes the boundary between mathematical scenarios and empirical measurement explicit. First, all state variables are dimensionless indices in the present calculations, and any empirical interpretation requires separately reported raw variables and reference scales. Second, forest condition is included directly in the objective functional to represent the conservation preference. Third, the invariant region is derived from valid comparison bounds. Fourth, the numerical procedure, sensitivity analysis, and alternative discretization cross-check are documented without treating the resulting candidate controls as a certificate of global numerical optimality.

The contribution is model-specific and is stated relative to the uncontrolled framework of [8]: First, the present study introduces two bounded intervention channels with distinct mechanisms: environmental education increases the removal rate of population pressure, whereas mining restriction increases the removal rate of mining activity. Second, it proves positivity, local well-posedness and global continuation in a valid control-independent bounding region. Third, for constant admissible interventions, it derives an explicit positive equilibrium and a control-dependent feasibility threshold. Fourth, it establishes a new model-specific comparative-statics theorem: wherever that positive equilibrium exists, the equilibrium forest index is strictly increasing in either constant intervention. Fifth, it provides an executable implementation, an extended saturation sensitivity analysis, a three-grid convergence check, and a four-start direct single-shooting control-parameterization diagnostic. These results are new for the present controlled forest–population-pressure–mining system. They are not claimed as a new general optimal-control existence theorem or as empirical estimates for a geographical region.

Environmental education and mining restriction are modeled as structural intervention channels rather than empirically estimated program or legal effects. References [11–15] provide contextual literature on environmental education, mining, and governance; they are not used to estimate the intervention multipliers θ_E and μ_R. The numerical results therefore quantify trade-offs among model indices and effort penalties only. They do not quantify employment, profit, tax revenue, social welfare, or a causal policy effect in a particular geographical region.

Section 2 defines the state system, the index interpretation, and the calibration boundary. Section 3 establishes the mathematical properties, constant-control equilibrium result, and reproducible illustrative numerical experiments. Section 4 states conclusions and limitations that are consistent with the represented variables and numerical methods.

2. Methods

Let $F(t), N(t), P(t)$, and $M(t)$ denote dimensionless model indices of forest-resource condition, human population, population pressure, and mining activity, respectively, at time t. The word index does not mean that the present numerical values were calculated by dividing observed variables by reported reference values: no empirical normalization is performed in this study. For a future calibrated application, raw measures $\mathrm{F_{raw}}, \mathrm{N_{raw}}, \mathrm{P_{raw}}$, and $\mathrm{M_{raw}}$ could be nondimensionalized as $\mathrm{F} = \frac{\mathrm{F_{raw}}}{\mathrm{F_{ref}}}, \mathrm{N} = \frac{\mathrm{N_{raw}}}{\mathrm{N_{ref}}}, \mathrm{P} = \frac{\mathrm{P_{raw}}}{\mathrm{P_{ref}}}$, and $\mathrm{M} = \frac{\mathrm{M_{raw}}}{\mathrm{M_{ref}}}$, provided that the study reports the geographical boundary, observation period, data source, positive reference values, and the reproducible formula used to construct $\mathrm{P_{raw}}$. None of those empirical inputs is specified here. Consequently, F, N, P, M, L, K, and π are dimensionless quantities on an arbitrary illustrative scenario scale, not direct observations in trees ha^{-1}, persons km^{-2}, or km^2 and not empirically normalized measurements.

The controls $u_1(t)$ and $u_2(t)$ are dimensionless effort fractions constrained to $[0, 1]$. The multipliers θ_E and μ_R, each with unit year^{-1}, convert those fractions into additional modeled removal rates for P and M. They are assumed numerical multipliers for the illustrative scenarios and are not calibrated estimates of the effects of a particular education program or mining regulation.

$$\frac{dF}{dt} = F\left(r - \frac{r_0 F}{L}\right) - \gamma_1 M F - \gamma_2 N F \tag{1}$$

$$\frac{dN}{dt} = N\left(s - \frac{s_0 N}{K}\right) + \pi\gamma_2 N F \tag{2}$$

$$\frac{dP}{dt} = \lambda N - (\theta_0 + \theta_E u_1) P \tag{3}$$

$$\frac{dM}{dt} = \Lambda + \alpha P - (\mu_0 + \mu_R u_2) M \tag{4}$$

with the initial conditions,

$$F(0) = F_0, \quad N(0) = N_0, \quad P(0) = P_0, \quad M(0) = M_0. \tag{5}$$

System (1)-(5) encodes the specified structural assumptions: logistic self-limitation, nonlinear interactions, and control action through the removal channels in (3) and (4). These assumptions support mathematical analysis; they are not presented as empirically validated causal relationships for a specific forest region. The illustrative numerical settings are listed in Table 2.

Eq. (1) represents logistic forest-index growth with self-limitation scale parameter L and modeled losses associated with mining and population indices. Eq. (2) represents logistic population-index growth with self-limitation scale parameter K and the specified forest-associated contribution. The positive term $\pi\gamma_2 N F$ is inherited structurally from the source framework in [8] and represents a stylized forest-resource support feedback. The interaction $\gamma_2 N F$, which contributes to forest-resource depletion in Eq. (1), is assumed simultaneously to provide a limited population-support effect through access to land, forest-dependent livelihoods, food, fuelwood, ecosystem services, or related economic opportunities. The dimensionless coefficient π scales the fraction of this interaction that enters the population-growth equation. Therefore, the term does not imply that forest degradation generally causes population growth; it represents a model-specific assumption that access to forest resources can temporarily support population persistence or growth. In a location-specific application, this coupling would require independent empirical calibration and could alternatively be represented by a separate coefficient rather than being constrained to remain proportional to γ_2. Eq. (3) represents pressure generated by the population index and removed at a modeled rate. Eq. (4) represents baseline mining activity, pressure-associated mining activity, and modeled removal. All parameters are positive, while either intervention effort may be zero. The formulation is illustrative and is not calibrated to a specific forest region. Here, the baseline term $\theta_0 P$ represents background attenuation of population pressure that operates independently of environmental education and aggregates adjustment processes not separately resolved by the model. Therefore, with $u_1 = 0$, P can still decrease whenever $\theta_0 P > \lambda N$, education strengthens this existing removal channel. The human population affects mining activity indirectly through the pathway $N \to P \to M$: the term λN raises population pressure in Eq. (3), and αP then raises mining activity in Eq. (4), N does not enter the mining equation directly.

Table 1: State variables, units, and calibration status

Symbol	Model interpretation	Unit/status in this study	Raw proxy and requirements for a future calibration
F	Forest-resource condition index	Dimensionless model index; not empirically normalized	Example raw proxy: tree density [trees ha^{-1}]; report F_{ref}, source, region, and period before calibration.
N	Human-population index	Dimensionless model index; not empirically normalized	Example raw proxy: population density [persons km^{-2}]; report N_{ref} source, region, and period.
P	Population-pressure index	Dimensionless model index; not empirically normalized	Define a reproducible raw pressure measure, P_{ref}, source, region, and period.
M	Mining-activity index	Dimensionless model index; not empirically normalized	Example raw proxy: mine-area footprint [km^2] in a defined region; report M_{ref}, source, and period.
u_1	Environmental-education effort	Dimensionless fraction in $[0, 1]$	No direct physical conversion is assigned in this illustrative model.
u_2	Mining-restriction effort	Dimensionless fraction in $[0, 1]$	No direct physical conversion is assigned in this illustrative model.

Because all model states are dimensionless scenario variables, every coefficient multiplying a state or state product is expressed in year^{-1}, whereas L, K, π, the state variables, and the control fractions are dimensionless. The figures and tables consequently report model indices rather than observed tree density, population density, mine area, or measured intervention intensity. A calibrated application would require the raw variables and reference scales listed in Table 1. The objective weights have arbitrary objective-score units, so J is reported in objective-score–years, neither quantity is monetary.

The structural baseline values $r, r_0, \gamma_1, \gamma_2, s, K, s_0, \pi, \lambda, \theta_0, \Lambda, \alpha$, and μ_0 are adapted from the arbitrary illustrative parameter set reported in [8], they are not empirical estimates. The present study deliberately uses $L = 50$ as its baseline scenario scale, whereas [8] used $L = 20$. To make that departure transparent, $L = 20$ is included in the sensitivity analysis. The new intervention multipliers and objective weights are assumed values introduced by this study.

Table 2: Illustrative baseline parameter values and provenance

No.	Symbol	Description	Value	Unit	Origin/status
1	L	Forest-index scaling parameter in the self-limitation term	50	dimensionless	Illustrative scale chosen here, [8] used 20, which is tested in Table 7.
2	r	Intrinsic growth rate of forest index	1	year^{-1}	Adapted from the arbitrary illustrative set in [8], not empirically estimated.

No.	Symbol	Description	Value	Unit	Origin/status
3	r_0	Forest self-limitation rate	2	year^{-1}	Adapted from the arbitrary illustrative set in [8], not empirically estimated.
4	γ_1	Mining-associated forest-depletion coefficient	0.01	year^{-1}	Adapted from the arbitrary illustrative set in [8], not empirically estimated.
5	γ_2	Population-associated forest-depletion coefficient	0.01	year^{-1}	Adapted from the arbitrary illustrative set in [8], not empirically estimated.
6	s	Intrinsic growth rate of population index	1	year^{-1}	Adapted from the arbitrary illustrative set in [8], not empirically estimated.
7	K	Population-index scaling parameter in the self-limitation term	50	dimensionless	Adapted from the arbitrary illustrative set in [8], not empirically estimated.
8	s_0	Population-index self-limitation rate	2	year^{-1}	Adapted from the arbitrary illustrative set in [8], not empirically estimated.
9	π	Forest-associated population-response coefficient	0.01	dimensionless	Adapted from the arbitrary illustrative set in [8], not empirically estimated.
10	λ	Population-pressure generation rate	1	year^{-1}	Adapted from the arbitrary illustrative set in [8], not empirically estimated.
11	θ_0	Natural removal rate of population pressure	4	year^{-1}	Adapted from the arbitrary illustrative set in [8], not empirically estimated.
12	Λ	Constant mining-activity input rate	5	year^{-1}	Source symbol in [8], renamed to avoid collision with Λ; illustrative.
13	α	Pressure-associated mining-activity input rate	0.3	year^{-1}	Adapted from the arbitrary illustrative set in [8], not empirically estimated.
14	μ_0	Baseline removal rate applied to mining activity	0.2	year^{-1}	Adapted from the arbitrary illustrative set in [8], not empirically estimated.
15	θ_E	Education multiplier for P removal	1	year^{-1}	New assumed structural multiplier; not a measured program effect.
16	μ_R	Restriction multiplier for M removal	1	year^{-1}	New assumed structural multiplier; not a measured policy effect.
17	A_1	Relative forest-index reward weight	5	score	Assumed relative preference weight.
18	A_2	Relative pressure-index penalty weight	10	score	Assumed relative preference weight.
19	A_3	Relative mining-index penalty weight	10	score	Assumed relative preference weight.

No.	Symbol	Description	Value	Unit	Origin/status
20	B_1	Quadratic education-effort weight	15	score	Assumed relative preference weight.
21	B_2	Quadratic restriction-effort weight	15	score	Assumed relative preference weight.
22	u_1	Environmental-education control	$[0, 1]$	dimensionless	Specified admissible-control bound.
23	u_2 *	Mining-restriction control	$[0, 1]$	dimensionless	Specified admissible-control bound.

For all baseline numerical experiments, the initial state is $X_0 = (F_0, N_0, P_0, M_0) = (25, 25, 6, 25)$. This fully specifies the illustrative numerical scenario, but it does not represent an observed state in a named location or physical measurement unit.

3. Results and Discussion

To present the findings systematically, this section begins by establishing the fundamental mathematical properties of the controlled system, followed by the derivation of equilibrium behavior and the numerical solution of the optimal control problem.

3.1. Results

3.1.1. Existence and uniqueness of solutions

Theorem 1. *For each measurable control $u = (u_1, u_2)$ satisfying $0 \leq u_i(t) \leq 1$ almost everywhere and for each nonnegative initial state, system (1)-(4) admits a unique maximal Carathéodory solution on an interval $[0, t_{\max})$.*

Proof. Let $X = (F, N, P, M)^{\mathrm{T}}$ and write the system as $X' = f(t, X, u(t))$. For a fixed admissible control, each component of f is continuous in X and polynomial in the state variables. On every bounded subset of $\mathbb{R}^4$, the Jacobian of f with respect to X is uniformly bounded for $u \in [0, 1]^2$. Hence f is locally Lipschitz in X uniformly in t and measurable in t through $u(t)$. The Carathéodory existence-and-uniqueness theorem yields a unique local absolutely continuous solution. This establishes local well-posedness only; the subsequent invariant-region analysis establishes global continuation. □

3.1.2. Positive invariant region

Theorem 2. *If $X(0) \in \mathbb{R}^4_+$, then the solution $X(t)$ remains in $\mathbb{R}^4_+$ throughout its interval of existence.*

Proof. At $F = 0$ and $N = 0$, the first and second right-hand sides equal zero. At $P = 0$, the derivative satisfies $P' = \lambda N \geq 0$. At $M = 0$, the derivative satisfies $M' = \Lambda + \alpha P > 0$. Therefore, on each coordinate boundary of the nonnegative orthant, the vector field is tangent to the boundary or points into the orthant. The variation of constants representations for P and M contain nonnegative integrands, and the multiplicative forms of the F and N equations preserve nonnegativity. Uniqueness consequently prevents any nonnegative solution from crossing a coordinate boundary into the negative orthant. □

3.1.3. A valid positively invariant region and global continuation

The conditions $F(t) \leq L$ and $N(t) \leq K$ do not follow from (1)-(2) in general because the interaction terms and logistic coefficients do not make L and K invariant upper bounds. The following comparison bounds provide valid upper bounds for the controlled system.

$$F_{\max} = \max\left\{F_0, \frac{rL}{r_0}\right\}, \tag{6}$$

$$N_{\max} = \max\left\{N_0, \frac{K(s + \pi\gamma_2 F_{\max})}{s_0}\right\}, \tag{7}$$

$$P_{\max} = \max\left\{P_0, \frac{\lambda N_{\max}}{\theta_0}\right\}, \tag{8}$$

$$M_{\max} = \max\left\{M_0, \frac{\Lambda + \alpha P_{\max}}{\mu_0}\right\}, \tag{9}$$

$$\Omega = [0, F_{\max}] \times [0, N_{\max}] \times [0, P_{\max}] \times [0, M_{\max}]. \tag{10}$$

For a fixed initial condition $X_0 = (F_0, N_0, P_0, M_0)^{\mathrm{T}}$, the bounds in (6)-(9) and the region in (10) depend on X_0; write this region as $\Omega(X_0)$. The order of F, N, P, and M in $\Omega(X_0)$ matches the state vector $X = (F, N, P, M)^{\mathrm{T}}$.

Theorem 3. *Fix a nonnegative initial condition X_0 and let $\Omega(X_0)$ be the region defined by (6)–(10). The solution that starts at X_0 remains in $\Omega(X_0)$ on its interval of existence. Consequently, the maximal solution in Theorem 1 extends to every finite interval $[0, T]$.*

Proof. Positivity is supplied by Theorem 2. It remains to verify the vector field on every upper face of $\Omega(X_0)$. If $F = F_{\max}$, then $F' \leq F_{\max}\left(r - \frac{r_0 F_{\max}}{L}\right) \leq 0$. If $N = N_{\max}$, then $N' \leq N_{\max}\left[s + \pi\gamma_2 F_{\max} - \frac{s_0 N_{\max}}{K}\right] \leq 0$. If $P = P_{\max}$, then $P' \leq \lambda N_{\max} - \theta_0 P_{\max} \leq 0$. If $M = M_{\max}$, then $M' \leq \Lambda + \alpha P_{\max} - \mu_0 M_{\max} \leq 0$. The lower faces are protected by positivity. Thus the solution that begins at X_0 cannot leave $\Omega(X_0)$. Since $\Omega(X_0)$ is compact, the standard continuation criterion excludes finite-time blow-up and extends the solution to every prescribed finite horizon. ☐

The proof sequence is essential. Theorem 1 establishes local existence and uniqueness, Theorem 2 establishes positivity, and Theorem 3 establishes a control-independent positively invariant region $\Omega(X_0)$ and global continuation. No theorem relies on a result that is established later in the analysis.

3.1.4. Constant-control equilibria and control-dependent threshold

The time-varying optimal-control problem need not possess a time-independent equilibrium. To identify the analytical role of each intervention channel, consider constant admissible controls $\bar{u} = (\bar{u}_1, \bar{u}_2) \in [0, 1]^2$. Define,

$$d_1 = \theta^0 + \theta_E \bar{u}_1, \tag{11}$$

$$d_2 = \mu_0 + \mu_R \bar{u}_2, \tag{12}$$

$$a(\bar{u}) = r - \frac{\gamma_1}{d_2}\left[\Lambda + \frac{\alpha\lambda K s}{d_1 s_0}\right] - \frac{\gamma_2 K s}{s_0}, \tag{13}$$

$$b(\bar{u}) = \frac{r_0}{L} + \frac{\gamma_1 \alpha\lambda K \pi\gamma_2}{d_1 d_2 s_0} + \frac{\gamma_2 K \pi\gamma_2}{s_0}. \tag{14}$$

Proposition 1. *If $a(\bar{u}) > 0$, the controlled system with $u(t) = \bar{u}$ has the unique positive equilibrium $F^* = \frac{a(\bar{u})}{b(\bar{u})}$, $N^* = \frac{K(s+\pi\gamma_2 F^*)}{s_0}$, $P^* = \frac{\lambda N^*}{d_1}$, and $M^* = \frac{(\Lambda+\alpha P^*)}{d_2}$.*

Proof. At an equilibrium, the P and M equations give $P^* = \frac{\lambda N^*}{d_1}$ and $M^* = \frac{(\Lambda+\alpha P^*)}{d_2}$. The positive N equation gives $N^* = \frac{K(s+\pi\gamma_2 F^*)}{s_0}$. Substitution of these relations into the positive F equation yields $a(\bar{u}) - b(\bar{u})F^* = 0$. All coefficients in $b(\bar{u})$ are positive, so $b(\bar{u}) > 0$; hence $a(\bar{u}) > 0$ is exactly the condition giving the stated unique positive equilibrium. □

Corollary 1 (model-specific comparative statics)**.** *On any part of the constant-control domain where $a(\bar{u}) > 0$, the equilibrium forest component $F^*(\bar{u})$ is strictly increasing in each intervention. For interior controls, $\frac{\partial F^*}{\partial \bar{u}_i} > 0$, $i = 1, 2$, the corresponding one-sided monotonicity holds at the endpoints.*

Proof. Because all parameters are positive, direct differentiation gives; $\frac{\partial a}{\partial \bar{u}_1} = \frac{\gamma_1\alpha\lambda K s\theta_E}{d_1^2 d_2 s_0} > 0$, $\frac{\partial a}{\partial \bar{u}_2} = \frac{\gamma_1\mu_R\left(\Lambda+\frac{\alpha\lambda K s}{d_1 s_0}\right)}{d_2^2} > 0$, $\frac{\partial b}{\partial \bar{u}_1} = -\frac{\gamma_1\alpha\lambda K\pi\gamma_2\theta_E}{d_1^2 d_2 s_0} < 0$, and $\frac{\partial b}{\partial \bar{u}_2} = -\frac{\gamma_1\alpha\lambda K\pi\gamma_2\mu_R}{d_1 d_2^2 s_0} < 0$. Therefore, $\frac{\partial F^*}{\partial \bar{u}_i} = \frac{\left(\frac{\partial a}{\partial \bar{u}_i}\right)b - a\left(\frac{\partial b}{\partial \bar{u}_i}\right)}{b^2} > 0$, $i = 1, 2$ because $a > 0$ and $b > 0$. This proves the claim. The result concerns the model equilibrium and does not estimate the effect of an empirical policy. □

Education increases d_1 and therefore directly strengthens removal of population pressure, while mining restriction increases d_2 and directly strengthens removal of mining activity. The threshold $a(\bar{u}) > 0$ shows how these mechanisms enter feasibility of the positive equilibrium, and Corollary 1 gives their separate monotonic effects on the equilibrium forest index. Neither result is an empirical policy-effect estimate.

3.1.5. Optimal control problem

For a prescribed horizon $T > 0$, the admissible control set and the objective functional are defined by,

$$U_{ad} = \{u = (u_1, u_2) \in L^2(0, T; \mathbb{R}^2) : u(t) \in [0, 1]^2 \text{ for a.e. } t \in [0, T]\}, \tag{15}$$

$$J(u) = \int_0^T \left[A_P P + A_M M - A_F F + \frac{B_1}{2}u_1^2 + \frac{B_2}{2}u_2^2\right] dt. \tag{16}$$

The term $-A_F F$ rewards a larger forest index because the control problem minimizes J. The terms $A_P P$ and $A_M M$ penalize population pressure and mining activity, respectively, whereas B_1 and B_2 penalize intervention intensity. These coefficients express relative mathematical preferences only. Because the model contains no economic data, they do not represent monetary costs, profits, or welfare. The optimal-control problem seeks a control $u^* \in U_{ad}$ such that,

$$J(u^*) = \min_{u \in U_{ad}} J(u). \tag{17}$$

3.1.5.1 Existence of an optimal control

Theorem 4. *For each finite horizon T, problem (1)-(4) and (15)-(16) admits at least one optimal control u^* and an associated state trajectory in $\Omega(X_0)$.*

Proof. Let $U = [0,1]^2$ and let $\ell(X,u)$ denote the running integrand. The admissible set U_{ad} is nonempty, convex, norm closed, and bounded in $L^2([0,T],\mathbb{R}^2)$. Because L^2 is reflexive, U_{ad} is weakly sequentially compact. By Theorems 1–3, every admissible control generates a unique state trajectory in the compact region $\Omega(X_0)$. The vector field $f(X,u)$ is Carathéodory in time, continuous and affine in u, and bounded on $\Omega(X_0)\times U$. The running integrand ℓ is continuous, bounded below, and convex in u. For each fixed X define the velocity–cost epigraph $E(X) = \{(v,z)\in\mathbb{R}^4\times\mathbb{R} : \exists u\in U, v = f(X,u), z\geq \ell(X,u)\}$. It is closed because U is compact and f and ℓ are continuous. It is convex: if (v_i,z_i) is generated by u_i for $i=1,2$ and $0\leq\rho\leq 1$, choose $u_\rho = \rho u_1 + (1-\rho)u_2 \in U$. Affinity gives $f(X,u_\rho) = \rho v_1 + (1-\rho)v_2$, while convexity gives $\ell(X,u_\rho)\leq \rho z_1 + (1-\rho)z_2$. Thus $E(X)$ is closed and convex. The Filippov–Cesari existence theorem now applies and guarantees an optimal pair [16]. This verifies nonemptiness, compactness of the pointwise control set, state boundedness, continuity, affinity of the velocity, convexity of the running cost, and closed convexity of the velocity–cost epigraph required by the cited theorem. □

3.1.5.2 Pontryagin characterization

Let $\eta = (\eta_1,\eta_2,\eta_3,\eta_4)$ denote the adjoint vector. The extremal is normal: if the cost multiplier were zero, the free-terminal-state condition $\eta(T) = 0$ and the resulting homogeneous adjoint system would imply $\eta = 0$, contradicting the nontriviality condition. The multiplier may therefore be set to one. The Hamiltonian is,

$$\mathcal{H} = A_P P + A_M M - A_F F + \frac{B_1}{2}u_1^2 + \frac{B_2}{2}u_2^2 + \eta_1 f_1 + \eta_2 f_2 + \eta_3 f_3 + \eta_4 f_4, \tag{18}$$

The functions f_i, $i = 1,2,3,4$, denote the right-hand sides of (1)-(4). Differentiating $\mathcal{H}$ with respect to u_1 and u_2, together with strict convexity of $\mathcal{H}$ in the controls, yields the unconstrained stationary controls. Projection of those controls onto $[0,1]$ gives (19)-(20).

$$u_1^* = \mathrm{Proj}_{[0,1]}\left(\frac{\eta_3\theta_E P}{B_1}\right), \tag{19}$$

$$u_2^* = \mathrm{Proj}_{[0,1]}\left(\frac{\eta_4\mu_R M}{B_2}\right), \tag{20}$$

Here, $\mathrm{Proj}_{[0,1]}(z) = \min\{1,\max\{0,z\}\}$. The state equations are (1)-(4) with $u = u^*$. The adjoint system follows from $\eta' = -\frac{\partial\mathcal{H}}{\partial x}$ and is given by (21)-(25).

$$\eta_1' = A_F - \eta_1\left(r - \frac{2r_0 F}{L} - \gamma_1 M - \gamma_2 N\right) - \eta_2\pi\gamma_2 N, \tag{21}$$

$$\eta_2' = \eta_1\gamma_2 F - \eta_2\left(s - \frac{2s_0 N}{K} + \pi\gamma_2 F\right) - \eta_3\lambda, \tag{22}$$

$$\eta_3' = \eta_3(\theta_0 + \theta_E u_1) - \eta_4\alpha - A_P, \tag{23}$$

$$\eta_4' = \eta_1\gamma_1 F + \eta_4(\mu_0 + \mu_R u_2) - A_M, \tag{24}$$

$$\eta_i(T) = 0, \quad i = 1,2,3,4. \tag{25}$$

Equations (1)-(4), (21)-(25), and the initial and terminal conditions form the optimality system used in the numerical calculations. The terminal conditions follow because the terminal state is free and the objective contains no terminal cost.

3.1.6. Reproducible numerical procedure

The numerical analysis used a forward–backward sweep method with fourth-order Runge–Kutta integration to compute a stationary candidate satisfying the stated optimality system. At all

4,001 baseline grid nodes, the active controls were initialized as $u_1^{(0)}(t) = u_2^{(0)}(t) = 0.5$, in a one-control or no-control scenario, each inactive control was fixed identically at zero. At iteration k, the state system was integrated forward, the adjoint system was integrated backward from $\eta(T) = 0$, projected candidate controls were computed from (19)-(20), and the relaxed update (26) was applied. A maximum of 3,000 sweep iterations was imposed. At each RK4 midstage, state and control inputs are the arithmetic averages of the two adjacent grid-node values.

$$u^{(k+1)}(t) = 0.5\tilde{u}^{(k+1)}(t) + 0.5u^k(t), \quad k = 0, 1, \ldots, \tag{26}$$

where $\tilde{u}^{(k+1)}$ denotes the unrelaxed candidate computed from (19)-(20). The baseline uses $T = 40$ years and $\Delta t = 0.01$ year, i.e., 4,000 time intervals. Iteration stops when,

$$\max_{t\in[0,T]} \|u^{(k+1)}(t) - u^k(t)\|_\infty < 10^{-7}, \tag{27}$$

The baseline two-control sweep met the stopping criterion after 25 iterations. The executable file `Supplementary_Code_Forest_Optimal_Control.py` reproduces the baseline, sensitivity, grid-convergence, and multi-start calculations. The reported controls are numerical stationary candidates; the direct single-shooting control-parameterization check supports local consistency but does not establish global numerical optimality. The composite trapezoidal rule is used for J and all reported time-integral or time-mean quantities. The 40-year baseline horizon was selected as an illustrative long-term interval that allows transient responses to develop and can be compared with the 20-year and 60-year horizons in the sensitivity analysis, it is not a location-specific policy period.

Table 3: Numerical implementation settings

Item	Baseline setting	Purpose
Integrator	Fourth-order Runge–Kutta	State and costate integration
Time horizon and step	$T = 40, \Delta t = 0.01$	4,000 integration intervals (4,001 grid nodes)
Baseline initial state	$X_0 = (25, 25, 6, 25)$	Fully specified initial condition
Initial controls	$u_1^{(0)} = u_2^{(0)} = 0.5$ at every node	Inactive controls are fixed at zero
Update	Relaxation 0.5, projection to $[0, 1]$	Prevents unstable direct updates and enforces bounds
Stopping rule	Maximum control change $< 10^{-7}$	Maximum 3,000 iterations
Observed iterations	25	Baseline two-control case
Alternative cross-check	40 piecewise-constant control pairs; RK4 0.1-year substeps, SLSQP, variational gradient, $f_{tol} = 10^{-8}$, max 100 iterations, four starts	Direct single-shooting control parameterization, local diagnostic only

Table 4: Grid-convergence check for the baseline two-control candidate

Δt	J	$F(40)$	$P(40)$	$M(40)$	Iterations
0.020	1,427.958084	17.362732	5.675394	6.230808	25
0.010	1,427.948807	17.362759	5.675138	6.230188	25
0.005	1,427.946486	17.362762	5.675074	6.230104	25

Across $\Delta t = 0.02$, 0.01 and 0.005 year, the maximum terminal-state difference is below 0.001 and the maximum objective difference is below 0.012. This supports discretization stability of the baseline sweep candidate at the precision used in the result tables.

All vertical axes display dimensionless model indices; the horizontal axis is time in years. Panel-specific vertical ranges are used to show within-variable differences; values should be compared within each panel, not by visual slope across panels. Fig. 2 presents the corresponding numerically

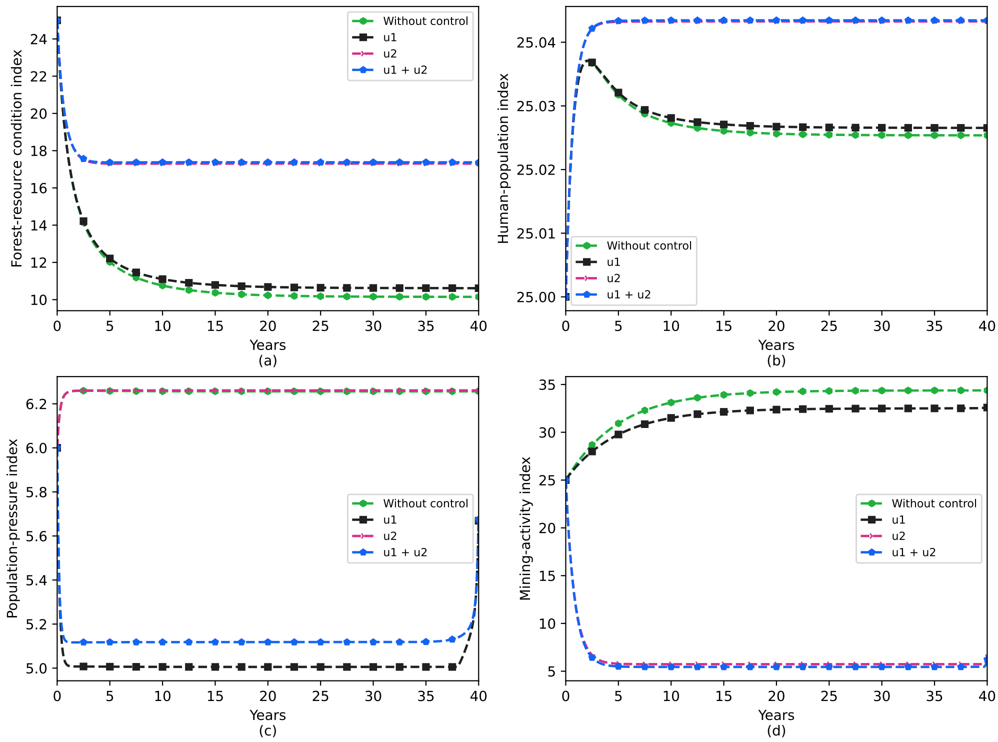

Fig. 1: State-index profiles under no control and the numerically computed candidate-control scenarios u_1, u_2, and $(u_1 + u_2)$.

computed control profiles. The vertical axis is a dimensionless control-effort fraction. The profiles describe allocation within the specified model, selected weights, bounds, and numerical procedure; they are not estimated real-world program intensities.

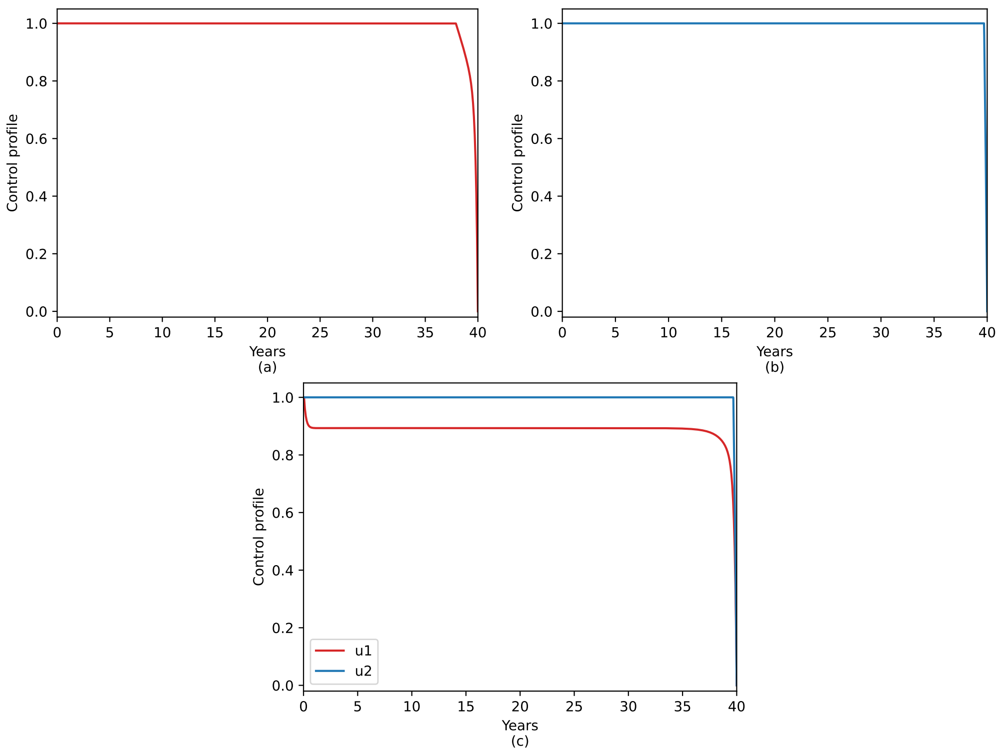

Fig. 2: Numerically computed candidate-control profiles. The vertical axis is the dimensionless control-effort fraction and the horizontal axis is time in years.

3.1.7. Objective function values

Table 5 reports the values of the objective functional in (16) for the four intervention scenarios, as reproduced using the executable code provided in `Supplementary_Code_Forest_Optimal_Control.py`. The no-control value is evaluated with $u = (0, 0)$. Under the selected relative weights, the two-control candidate yields the lowest computed aggregate objective among the four scenarios. This ranking is conditional on the specified objective functional and does not establish global numerical optimality or a ranking with respect to every individual endpoint.

Table 5: Objective functional values under the illustrative baseline

Scenario	J	**Reduction relative to no control**
Without control	$13,585.205$	-
u_1	$12,657.053$	6.832%
u_2	$1,768.848$	86.980%
$u_1 + u_2$	$1,427.949$	89.489%

3.1.8. Terminal state values and effectiveness

Table 6 reports terminal values at $t = 40$, and Table 7 reports changes relative to the uncontrolled baseline. Among the four reported scenarios, the two-control candidate has the largest $F(40)$, the smallest $M(40)$, and the lowest computed J. The education-only candidate has the smallest $P(40)$ among these scenarios. These endpoint comparisons must not be conflated with a separately posed terminal-state optimization problem or interpreted as an empirical policy ranking.

Table 6: State variables at the end of the simulation ($t = 40$)

Variable	**No control**	u_1	u_2	$u_1 + u_2$
$F(40)$	10.1491	10.6136	17.2946	17.3628
$N(40)$	25.0254	25.0265	25.0433	25.0434
$P(40)$	6.2563	5.6692	6.2608	5.6751
$M(40)$	34.3814	32.5897	6.4763	6.2302

Table 7: Effectiveness relative to the uncontrolled baseline

Measure	u_1	u_2	$u_1 + u_2$	**Interpretation**
Increase in $F(40)$	4.577%	70.406%	71.077%	Highest $F(40)$ among the four reported scenarios.
Reduction in $P(40)$	9.384%	-0.071%	9.290%	Lowest $P(40)$ among the four reported scenarios.
Reduction in $M(40)$	5.211%	81.163%	81.879%	Lowest $M(40)$ among the four reported scenarios.
Reduction in J	6.832%	86.980%	89.489%	Lowest computed J among the four reported scenarios.

3.1.9. Sensitivity analysis and alternative-method check

The sensitivity analysis examines the illustrative baseline weights, horizon, initial state, and forest self-limitation scale parameter for the two-control numerical candidate. For the rows with $T = 20$ and $T = 60$, the state columns in Table 8 report the corresponding terminal values $F(T)$, $P(T)$, and $M(T)$, rather than values evaluated at $t = 40$. The row $L = 20$ reproduces the value of L used in the source model [8], thereby making the selection of $L = 50$ in the present study transparent. Table 8 reports the terminal outcomes and mean control levels, whereas Table 9 presents the unweighted time averages of the state terms and squared-control terms common to all scenarios. Because changing an objective weight also changes the definition of the objective functional, J and J/T are not used for comparisons across different sensitivity rows. Here $I_F = \int_0^T F(t)\,dt$, $I_P = \int_0^T P(t)\,dt$, $I_M = \int_0^T M(t)\,dt$, $I_{u_1^2} = \int_0^T u_1^2(t)\,dt$, and $I_{u_2^2} = \int_0^T u_2^2(t)\,dt$, every mean in 8–11 is the corresponding composite-trapezoidal integral divided by T.

Table 8: Sensitivity of the two-control numerical candidate

Test	$F(T)$	$P(T)$	$M(T)$	**Mean** u_1	**Mean** u_2
$B_1 = B_2 = 7.5$	17.381	5.376	5.801	0.998	0.998
$B_1 = B_2 = 15$ (baseline)	17.363	5.675	6.230	0.886	0.996
$B_1 = B_2 = 30$	17.300	5.916	7.056	0.518	0.993
$T = 20$	17.363	5.675	6.230	0.879	0.993
$T = 60$	17.363	5.675	6.230	0.888	0.998
$X_0 = (20, 20, 4, 20)$	17.363	5.675	6.230	0.881	0.996
$X_0 = (30, 30, 8, 30)$	17.363	5.675	6.230	0.889	0.996
$L = 20$	6.948	5.670	6.233	0.876	0.996
$L = 40$	13.892	5.673	6.231	0.883	0.996
$L = 60$	20.833	5.677	6.229	0.889	0.996

Table 9: Objective-independent time-average components for Table 8 scenarios

Test	I_F/T	I_P/T	I_M/T	$I_{u_1^2}/T$	$I_{u_2^2}/T$
$B_1 = B_2 = 7.5$	17.509	5.014	5.828	0.997	0.998
$B_1 = B_2 = 15$ (baseline)	17.503	5.127	5.857	0.788	0.995
$B_1 = B_2 = 30$	17.478	5.543	5.965	0.269	0.990
$T = 20$	17.628	5.137	6.268	0.777	0.990
$T = 60$	17.461	5.124	5.720	0.791	0.997
$X_0 = (20, 20, 4, 20)$	17.427	5.093	5.744	0.779	0.995
$X_0 = (30, 30, 8, 30)$	17.560	5.157	5.969	0.793	0.995
$L = 20$	7.233	5.132	5.858	0.771	0.995
$L = 40$	14.115	5.129	5.857	0.782	0.995
$L = 60$	20.865	5.126	5.856	0.793	0.995

Table 10 varies one objective weight at a time and reports terminal states, time-mean controls, and the saturation fraction, $S_2 = \frac{1}{T}\int_0^T \mathbb{1}_{\{u_2(t)\geq 0.99\}}\, dt$. Table 11 reports the corresponding unweighted time-average components $\frac{I_F}{T}$, $\frac{I_P}{T}$, $\frac{I_M}{T}$, $\frac{I_{u_1^2}}{T}$, and $\frac{I_{u_2^2}}{T}$, whose definitions remain consistent across all rows. The extended values $B_2 = 60$ and $B_2 = 150$ are included to examine whether the near-unity baseline value of u_2 is structurally forced or results from the selected intervention-cost weight. The objective values J and J/T are not compared across rows because changing an objective weight also changes the definition of the objective functional.

Table 10: One-at-a-time sensitivity to objective-function weights

Test	$F(40)$	$P(40)$	$M(40)$	**Mean** u_1	**Mean** u_2	S_2
$A_F = 2.5$	17.362	5.675	6.234	0.879	0.996	0.992
$A_F = 10$	17.364	5.675	6.224	0.901	0.996	0.992
$A_P = 5$	17.343	5.903	6.311	0.606	0.996	0.992
$A_P = 20$	17.372	5.380	6.171	0.998	0.996	0.992
$A_M = 5$	17.323	5.684	6.948	0.822	0.993	0.982
$A_M = 20$	17.378	5.658	5.843	0.991	0.998	0.996
$B_1 = 7.5$	17.372	5.376	6.171	0.998	0.996	0.992
$B_1 = 30$	17.337	5.917	6.325	0.518	0.997	0.992
$B_2 = 7.5$	17.372	5.676	5.860	0.886	0.998	0.996
$B_2 = 30$	17.324	5.674	6.962	0.886	0.992	0.981
$B_2 = 60$	17.124	5.674	8.335	0.894	0.930	0.070
$B_2 = 150$	16.577	5.673	10.775	0.939	0.658	0.020

Table 11: Objective-independent time-average components for Table 10 scenarios

Test	I_F/T	I_P/T	I_M/T	$I_{u_1^2}/T$	$I_{u_2^2}/T$
$A_F = 2.5$	17.502	5.135	5.859	0.774	0.995
$A_F = 10$	17.504	5.112	5.853	0.815	0.995
$A_P = 5$	17.485	5.438	5.933	0.368	0.995
$A_P = 20$	17.509	5.014	5.830	0.997	0.995
$A_M = 5$	17.499	5.195	5.880	0.678	0.990
$A_M = 20$	17.509	5.020	5.829	0.985	0.998
$B_1 = 7.5$	17.509	5.014	5.830	0.997	0.995
$B_1 = 30$	17.478	5.544	5.959	0.269	0.995
$B_2 = 7.5$	17.503	5.127	5.856	0.788	0.998
$B_2 = 30$	17.503	5.127	5.863	0.788	0.989
$B_2 = 60$	17.440	5.119	6.145	0.801	0.872
$B_2 = 150$	17.012	5.072	7.938	0.885	0.441

At $B_2 = 30$, mean u_2 is 0.992 and $S_2 = 0.981$. Increasing B_2 to 60 and 150 lowers mean u_2 to 0.930 and 0.658 and lowers S_2 to 0.070 and 0.020, respectively. Thus the upper-bound behavior is not hard-wired into the algorithm: it relaxes when mining-restriction effort is penalized more strongly. The associated increase in $M(40)$ makes the effort-state trade-off explicit.

As a multi-start cross-check with an alternative discretization, the baseline two-control problem was solved by direct control parameterization with single shooting: 40 piecewise-constant control pairs were optimized while the states were integrated with 0.1-year RK4 substeps. SLSQP used a variational-equation gradient, $f_{tol} = 10^{-8}$, and at most 100 iterations. Four deterministic initial vectors were used: a downsampled sweep solution, all zeros, all ones, and a pseudo-random vector with seed 20260731. All four runs converged to $J = 1,429.007$ (to three decimals), compared with $J = 1,427.949$ for the sweep; the relative difference is 0.074%. The starts required 14, 22, 20, and 24 iterations, respectively. This demonstrates local agreement across the reported discretizations and starts, but it is not evidence of a global numerical optimum.

Table 12: Multi-start direct single-shooting control-parameterization cross-check

Method	**Objective** J	**Iterations**	**Difference from sweep**
Forward-backward sweep (RK4)	$1,427.949$	25	Reference
Single shooting: sweep-downsampled start	$1,429.007$	14	0.074%
Single shooting: zero start	$1,429.007$	22	0.074%
Single shooting: one start	$1,429.007$	20	0.074%
Single shooting: pseudo-random start (seed 20260731)	$1,429.007$	24	0.074%

3.2. Discussion

Within the specified model, mining restriction has the strongest direct pathway to the forest index because u_2 increases the removal rate of M and M appears directly in the forest-depletion term $\gamma_1 MF$. Environmental education acts through P and hence affects F indirectly. These statements describe the model structure, not an empirical estimate of the relative effectiveness of actual education and mining-regulation policies.

The population index remains close to 25 in all scenarios. The controls enter the population equation only indirectly through the forest index, and the coupling coefficient $\pi\gamma_2 = 10^{-4}$ is small under the illustrative baseline. Because the population-support coefficient is specified as $\pi\gamma_2$, the present model assumes that the forest-associated population response is proportional to the population-associated forest-depletion interaction. This coupling is inherited from [8] and may be relaxed in future work by introducing an independently estimated forest-to-population response coefficient. This model-specific result does not demonstrate that real populations are unaffected by environmental policies. Population pressure follows a different mechanism because u_1 acts directly on its removal rate and substantially reduces P. Mining restriction alone does not reduce P. The small negative value in Table 7 indicates that the terminal pressure index is marginally higher than the no-control value rather than an improvement.

The endpoint comparison requires a qualified interpretation. Among the four reported scenarios, the two-control candidate yields the lowest computed integral objective and improves the forest and mining endpoints, whereas the education-only candidate yields the smallest terminal pressure index. This does not imply that either strategy is optimal for a separately formulated terminal-pressure objective, for a different objective weight set, or for a real-world decision maker. The objective includes time-path and effort components that a single endpoint omits.

Fig. 2 and the baseline rows in Tables 8–11 show that u_2 remains close to one during most of the illustrative horizon. The extended B_2 analysis demonstrates that this saturation is weight-dependent: stronger effort penalties move u_2 decisively into the interior. Accordingly, the baseline profile is a property of the selected coefficients, weights, bounds, and numerical candidate; it is not a recommendation that a real regulator impose maximal mining restrictions.

The present model excludes revenue, employment, mining profit, enforcement budgets, household welfare, spatial heterogeneity, and observations from a specific forest region. It therefore cannot quantify a balance between forest conservation and economic growth or support a calibrated real-world policy recommendation. Its conclusions are restricted to internally consistent behavior of the dimensionless dynamic system and associated optimal-control problem. Calibration, uncertainty quantification, and explicit socioeconomic state variables are necessary extensions for location-specific policy analysis. Comparable forest–human interaction models have shown that uncertainty and sensitivity analyses can identify the parameters that most strongly influence conservation outcomes [17]. The mining-restriction control u_2 represents only a reduction in ongoing mining activity through the modeled removal term. It does not explicitly represent post-mining reclamation or reforestation, introducing a restoration state or a separate restoration control is a possible extension.

4. Conclusion

Based on the mathematical analysis and illustrative numerical scenarios, the following conclusions are supported:

a) This study formulates and analyzes a four-dimensional optimal-control model for dimensionless indices of forest condition, population, population pressure, and mining activity. The numerical values lie on an arbitrary illustrative scale and are not empirically normalized measurements. A future calibration would have to report the raw variables, reference values, study area, observation period, and data sources.

b) The analysis establishes local existence and uniqueness, positivity, a valid control-independent positively invariant region $\Omega(X_0)$, global continuation, and optimal-control existence. It also derives an explicit positive equilibrium and control-dependent feasibility threshold for constant admissible interventions. The new comparative-statics result proves that the positive equilibrium forest component is strictly increasing in either constant intervention wherever the equilibrium exists.

c) The formulation states the invariant-set order, terminal conditions, admissible-control space, normality of the Pontryagin extremal, and a closed convex velocity–cost epigraph for the Filippov–Cesari argument. Executable Supplementary Material S1 reproduces the experiments. Three time grids are consistent at the reported precision, and four direct single-shooting starts agree locally with the sweep candidate; neither check establishes global numerical optimality.

d) Under the illustrative baseline and among the four reported scenarios, mining restriction is the modeled direct pathway for reducing the mining index and improving the forest index. The two-control candidate yields the lowest computed weighted objective, the largest terminal forest index, and the smallest terminal mining index; the education-only candidate yields the smallest terminal pressure index. Extended sensitivity shows that near-unity u_2 is reduced when B_2 is increased. These findings remain conditional on the model structure, selected weights, and numerical method and are not calibrated economic, causal, or location-specific policy estimates.

CRediT Authorship Contribution Statement

Asmaidi: Conceptualization, Methodology, Formal Analysis, Software, Investigation, Writing – Original Draft. **Fatmawati**: Conceptualization, Supervision, Validation, Writing – Review & Editing. **Cicik Alfiniyah**: Validation, Supervision, Formal Analysis, Writing – Review & Editing.

Declaration of Generative AI and AI-assisted technologies

Generative AI tools were used exclusively for language refinement and grammar checking during manuscript preparation. The authors reviewed and edited all resulting text and assume full responsibility for the final manuscript.

Declaration of Competing Interest

The authors declare no competing interests.

Ethics Approval and Consent to Participate

This study did not involve human participants, personal data, animal subjects, or materials requiring ethical approval.

Funding and Acknowledgments

This research received no external funding. The authors acknowledge the support provided by the Department of Mathematics, Universitas Airlangga, and Universitas Mulawarman.

Data and Code Availability

No experimental or empirical dataset was generated or analyzed in this study. Supplementary Material S1 contains the executable Python source file `Supplementary_Code_Forest_Optimal_Control.py`, which reproduces the baseline scenarios, extended sensitivity calculations, the three-grid convergence check, the direct single-shooting diagnostic, and the generation of Figures Fig. 1 and Fig. 2. The source file accepts documented command-line arguments and records the pseudo-random seed used in the numerical calculations. All numerical scenarios are illustrative and do not represent a calibrated empirical dataset.

References

[1] Wondimagegn Mengist and Teshome Soromessa. “Assessment of forest ecosystem service research trends and methodological approaches at global level: a meta-analysis”. In: *Environmental Systems Research* 8.1 (2019), pp. 1–22. DOI: 10.1186/s40068-019-0150-4.

[2] Stefan Sorge, Carsten Mann, Christian Schleyer, Lasse Loft, Martin Spacek, Mónica Hernández-Morcillo, and Tatiana Kluvankova. "Understanding dynamics of forest ecosystem services governance: A socio-ecological-technical-analytical framework". In: *Ecosystem Services* 55.101427 (2022), pp. 1–21. DOI: 10.1016/j.ecoser.2022.101427.

[3] María Liliana Ávalos Rodríguez, Michael K McCall, José Juan Alvarado Flores, and Jorge Víctor Alcaraz Vera. "Understanding community perceptions of forest ecosystem services to motivate REDD+ actions: A case study of Jalisco, Mexico". In: *Trees, Forests and People* 24.101176 (2026), pp. 1–12. DOI: 10.1016/j.tfp.2026.101176.

[4] Mélanie Feurer, Jelena Markovic, Michael Starke, Jerylee Wilkes-Allemann, and Oliver Wolf. "Drivers of deforestation and forest degradation between 1990 and 2023-A global meta-analysis". In: *Environmental Science & Policy* 173.104242 (2025), pp. 1–11. DOI: 10.1016/j.envsci.2025.104242.

[5] Xiaoxin Zhang, Bin Chen, Jiafu An, Chen Lin, and Peng Gong. "Overlooked deforestation from global mining activities in the 21st century". In: *Nature Communications* 17.804 (2025), pp. 1–10. DOI: 10.1038/s41467-025-67501-1.

[6] Stefan Giljum, Victor Maus, Nikolas Kuschnig, Sebastian Luckeneder, Michael Tost, Laura J Sonter, and Anthony J Bebbington. "A pantropical assessment of deforestation caused by industrial mining". In: *Proceedings of the National Academy of Sciences* 119.38, e2118273119 (2022), pp. 1–7. DOI: 10.1073/pnas.2118273119.

[7] Mingzhu Qu, Chunrui Zhang, and Xingjian Wang. "Analysis of dynamic properties on forest restoration-population pressure model". In: *Mathematical Biosciences and Engineering* 17.4 (2020), pp. 3567–3581. DOI: 10.3934/mbe.2020201.

[8] Abhinav Tandon, Kumari Jyotsna, and Susanto Dey. "A mathematical model to investigate the impact of overgrowing population-induced mining on forest resources". In: *Environment, Development and Sustainability* 20.4 (2018), pp. 1499–1516. DOI: 10.1007/s10668-017-9950-8.

[9] Ibrahim M Fanuel, Damian Kajunguri, and Francis Moyo. "Modelling the Impact of Human Population and Its Associated Pressure on Forest Biomass and Forest-Dependent Wildlife Population". In: *Journal of Applied Mathematics* 2023.1 (2023), pp. 1–9. DOI: 10.1155/2023/4826313.

[10] Fatmawati Fatmawati, Faishal F Herdicho, Nurina Fitriani, Norma Alias, Mazlan Hashim, and Olumuyiwa J Peter. "Optimal control strategies for dynamical model of climate change under real data". In: *Journal of the Nigerian Society of Physical Sciences* 7.3, Art. no. 2572 (2025), pp. 1–11. DOI: 10.46481/jnsps.2025.2572.

[11] P Sari, T Purnomo, and E Hariyono. *Research trend of environmental education in science based on the Scopus database. IJORER: International Journal of Recent Educational Research, 4 (3), 296–308.* 2023. DOI: 10.46245/ijorer.v4i3.296.

[12] H Husamah, Hadi Suwono, Hadi Nur, and Agus Dharmawan. "Environmental education research in Indonesian Scopus indexed journal: A systematic literature review". In: *Jurnal Pendidikan Biologi Indonesia* 8.2 (2022), pp. 104–120. DOI: 10.22219/jpbi.v8i2.21041.

[13] Yang Xiang, Suping Peng, and Wenfeng Du. "Trends and frontiers in coal mine groundwater research: insights from bibliometric analysis". In: *Geomechanics and Geophysics for Geo-Energy and Geo-Resources* 9.1 (2023), pp. 1–26. DOI: 10.1007/s40948-023-00663-8.

[14] Muhamad Muhdar, Rikardo Simarmata, and Mohamad Nasir. "Legal policy preference for coal mining over other land use alternatives jeopardizes sustainability in Indonesia". In: *Journal of Land Use Science* 18.1 (2023), pp. 395–408. DOI: 10.1080/1747423X.2023.2264845.

[15] João Victor Menezes Cunha, Eric Pirard, and Thomas Drnek. "Resource accessibility and depletion assessments: bridging the gap between geospheric and anthropospheric mineral resources". In: *Mineral Economics* (2026), pp. 1–13. DOI: 10.1007/s13563-026-00599-x.

[16] Suzanne Lenhart and John T Workman. *Optimal control applied to biological models*. CRC press, 2007. DOI: 10.1201/9781420011418.

[17] Ibrahim M Fanuel, Silas Mirau, Damian Kajunguri, and Francis Moyo. "Conservation of forest biomass and forest–dependent wildlife population: Uncertainty quantification of the model parameters". In: *Heliyon* 9.6, e16948 (2023), pp. 1–18. DOI: 10.1016/j.heliyon.2023.e16948.